Raindrop Breakup in the Shock Layer of a High-Speed Vehicle

GEORGE D. WALDMAN* AND WILLIAM G. REINECKE*
Avco Systems Division, Wilmington, Mass.
AND
DONALD C. GLENN†
The Aerospace Corporation, San Bernardino, Calif.

The problem of predicting raindrop breakup effects in the shock layer of a high-speed vehicle is discussed. Relevant experimental data, obtained in a shock tube with shadowgraph and x-ray photography, are presented in the form of correlations of the nondimensional time to breakup with the Weber number, together with the drop mass variation and trajectory as a function of nondimensional time. The relationship between the experimental situation and the flight case is delineated for the stagnation and downstream conical-flow regions of a high-speed shock layer. Based on the experimental correlations, calculations are made of the impacting drop mass fractions, velocities, and impact angles for a vehicle traversing a rainstorm.

Introduction

IF a supersonic vehicle flying through the Earth's atmosphere traverses a rainstorm, the raindrops striking the body surface at high speed may cause serious damage. Figure 1 is a photograph of a conical model fired in a ballistic range through a simulated rainstorm. The darkened areas in the wake of the cone consist of crater ejecta and the remnants of drops which have struck the surface and been swept downstream. The damage to the surface of such vehicle is partially alleviated, however, by the presence of the flowfield. Because the relative velocity between the raindrops and the flow near the body is high, the drops are deflected away from the surface.

As shown in Fig. 1, the drops are also distorted and torn apart by the severe aerodynamic forces exerted on them in traversing the shock layer. The small droplets in the stripped material have diameters of 1–10 μ (as estimated by Ranger and Nicholls[1]) and hence tend to conform to the flow streamlines. As a result, in many situations of interest a considerable portion of the raindrops swept out by a high speed vehicle will never reach the vehicle surface.

Figure 2 is another photograph of a ballistic-range model, in this case a yawed cylinder, traversing a simulated rain field. Figure 3 is a blowup of four of the drops in the lower righthand field of Fig. 2. The flow relative to the drops is from the upper right to the lower left in the figure. The drops are noticeably flattened by the relative flow and there is an indication of material being stripped away. Figure 4 is a shadowgraph of a drop being broken up in a shock tube. Comparison of Figs. 3 and 4 suggests that the in-flight drop shattering phenomenon can be simulated very well by a shock-tube experiment.

Previous drop breakup calculations[2] based on the data of Ranger and Nicholls,[1] Nicholson,[3] and Engel[4] were limited to a determination of the initial diameter of the smallest drop which would survive passage through the shock layer and strike the surface. Subsequently, we have carried out a study[5,6] to determine experimentally the drop mass as a function of time after shock passage until complete breakup, and to determine analytically how the experimental results could be applied in a general manner to actual flight.

In this paper, primary emphasis is placed on the last item. The relationship between the experimental situation and the passage of drops through the high-speed shock layer is determined for both the blunt-nose region and the downstream conical-flow region. Dimensionless impact times are calculated for a number of flight conditions. Employing non-dimensional correlations of the experimental data reported in Refs. 5–7, calculations are made of the impacting drop mass fractions, velocities, and impact angles for a representative flight configuration at the altitude of maximum water content for a typical model rainstorm. The results of Ref. 2 are compared to these calculations and appropriate conclusions are drawn.

Experiments and Correlation of Data

In the experimental program,[5,6] both flash x-ray and single-frame shadowgraph photographs were taken of waterdrops falling in the test section of a 1½-in. shock tube shortly after shock passage. Data were taken for a range of drop diameters from 0.5 to 2.5 mm, which is representative of naturally occurring raindrops. Shock tube conditions included initial, driven tube pressure levels from 140 to 760 torr, and shock Mach numbers from 3 to 11. The range of the test was sufficient to provide a generally adequate coverage of the conditions to be expected during flight through a rainstorm, with the exception of drops smaller than 0,5 mm in diameter.[5–7]

Shadowgraph pictures of the disintegration of waterdrops in the test facility are shown in Figs. 4 and 5. The initial drop occupies only a fraction of the dark area shown on these shadowgraphs, and it is evident that water is being stripped from the drops and swept downstream in the form of mist. It is hypo-

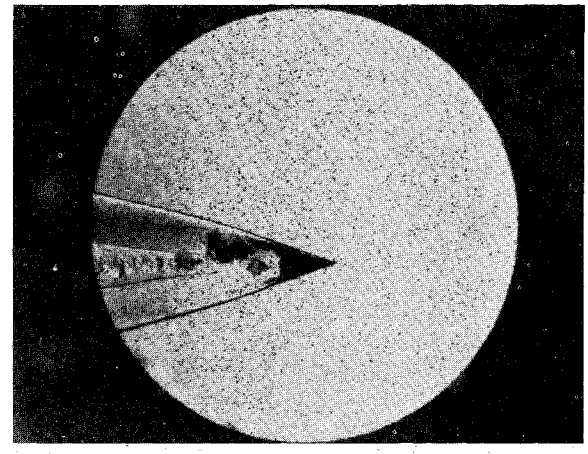

Fig. 1 Waterdrop impact on ballistic range conical model.

Received August 30, 1971; revision received April 7, 1972. This research was supported by the Space and Missile Systems Organization under Air Force Contract F04701-68-c-0035.
Index category: Multiphase Flows.
* Senior Consulting Scientist.
† Technical Staff.

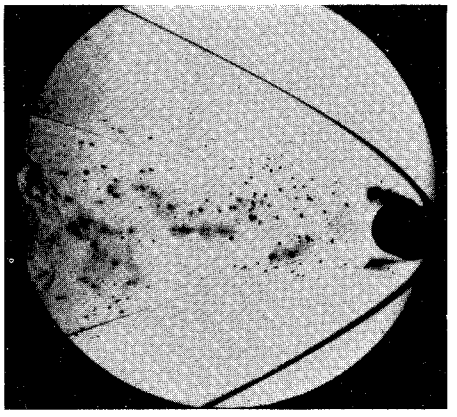

Fig. 2 Waterdrop impact on ballistic range cylindrical model.

thesized that in the early stages of disintegration (Fig. 4) the breakup process is continuous. On the forward face of the drop shown in Fig. 4 can be discerned a pattern of surface waves. In Ref. 5 it was shown that the amplitude of these waves grows exponentially, leading to the inference that the final stage of breakup shown in Fig. 5 is the result of the drop being torn apart by unstable waves. It was therefore postulated that two modes of breakup are important at high Mach numbers: first, a gradual stripping mode in which material is removed continuously, followed by a catastrophic mode in which the drop is rapidly torn apart.

To determine the amount of mass remaining in the distorted drop, obscured in shadowgraphs such as Fig. 4 and 5, a flash x-ray system was employed to obtain short exposure time radiograms of lead acetate saturated drops. A scanning microdensitometer was used to measure the distribution of film density of the x-radiograms, and the drop volumes were then obtained by numerically integrating the microdensitometer outputs. In this way, it was determined that the remaining unstripped water is confined initially to a lenticular volume at the front of the shadowgraph image, while the final disintegration process results in a random, unpredictable geometry.[5]

From data reported in Ref. 7, the trajectory of an initially motionless drop following shock passage can be correlated in dimensionless variables by the equation

$$X = 0.8\,T^2 \tag{1}$$

where

$$X = x/D_0$$
$$T = (tu_2/D_0)(\rho_2/\rho_L)^{1/2} \tag{2}$$

Here D_0 is the original drop diameter, ρ_2 the gas density and u_2 the flow velocity behind the shock (Fig. 5), ρ_L the liquid density, x the distance traveled by the drop in laboratory coordinates, and t the time after shock passage. Equation (1) corresponds to a constant acceleration trajectory with an average drag coefficient of about 2.1, based on the original cross-sectional area of the drop.

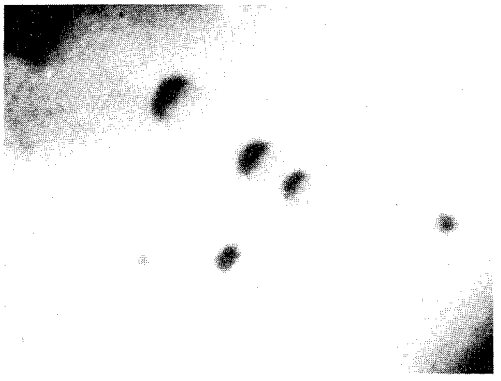

Fig. 3 Blowup of drop being broken up in Fig. 2.

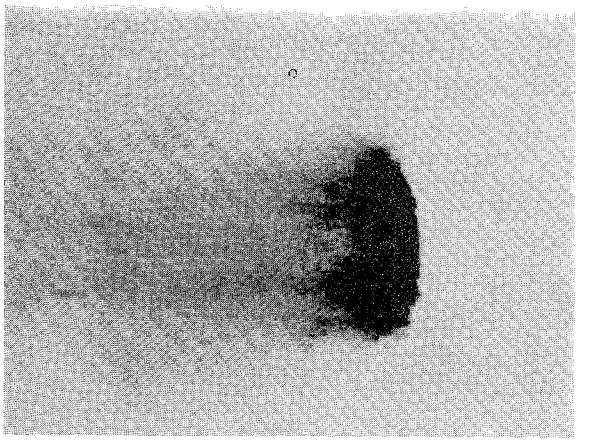

Fig. 4 Breakup of a waterdrop in a shock tube; early stage.

The dimensionless time elapsed between shock passage and the growth of the waves on the front surface of the drop to a given amplitude can be shown to depend inversely on the one-fourth power of the Weber number

$$W = \rho_2 u_2{}^2 D_0/\sigma_L \tag{3}$$

where σ_L is the surface tension of the drop liquid. The x-ray measurements of the dimensionless time to breakup T_C in this "catastrophic" mode are well correlated by the equation

$$T_C = 45\,W^{-1/4} \tag{4}$$

the exponent of which agrees with the theoretical result for wave amplification.

Transition from the stripping mode of breakup to catastrophic breakup occurs early in the tests at a shock Mach number of 11, at intermediate time at Mach 6, and at late time (if at all) at Mach 3. Hence the stripping mode is still important at the lower shock Mach numbers. The x-ray data suggest that the time for complete breakup due to stripping has the constant value

$$T_S = 3.5 \tag{5}$$

to a good approximation, independent of the shock Mach number. This is consistent with the earlier data of Nicholson.[3] The detailed data on the mass of the drop remnant as a function of time could be correlated by the empirical formula

$$m_S/m_0 = \tfrac{1}{2}(1 + \cos \pi T/T_S) \tag{6}$$

where m_0 is the initial mass of the drop.

Drop Breakup Calculations under Flight Conditions

Drop breakup calculations are divided into three parts. In the first part, the experimental correlation of drop deceleration in the shock tube is expressed in vehicle-fixed coordinates, and the nondimensional impact time is then computed as a function of

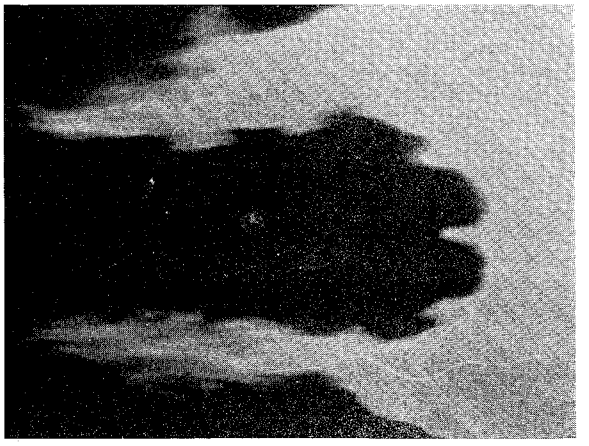

Fig. 5 Breakup of a waterdrop in a shock tube; final stage.

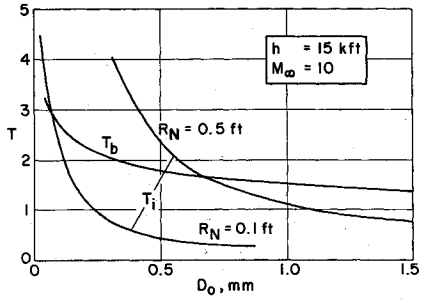

Fig. 6 Impact and breakup times for nose.

drop diameter. In the second part, the drop breakup criteria are used to ascertain the appropriate nondimensional breakup time as a function of drop diameter. Finally, the two times are compared in order to determine the fraction of drop mass entering the shock layer which strikes the vehicle surface as a function of drop diameter, and this function is integrated over the rainstorm drop mass distribution function to yield the net mass fraction impinging.

Two cases have been considered: the stagnation region of a blunt-nosed body and the conical region far downstream of the nose. In the stagnation region, a reasonable estimate is obtained by considering only the breakup of drops which traverse the stagnation streamline. Although drops which traverse other parts of the shock layer will experience somewhat different flow conditions, the stagnation streamline provides representative conditions and is simple to analyze. Furthermore, a direct analogy relates the stagnation streamline problem to the experimental conditions in the shock tube: In a high-speed shock layer, the flow conditions along the stagnation streamline are virtually uniform and hence similar to the uniform-flow region behind the shock wave in the shock tube. In the downstream region, the disturbance caused by the blunt nose tends to die out, and the flowfield becomes approximately conical. High-speed conical shock layers are also characterized by approximate uniformity, and similarity with experimental conditions can be established if it is observed that the relative flow velocity which acts on the drop is the component in the direction perpendicular to the bow shock wave.[2] Although it is possible to consider more complicated, nonuniform flowfields, this was not done for the present study.

In shock-tube coordinates, the distance between the shock wave and the drop is given by

$$s = u_s t - x \tag{7}$$

Since

$$\rho_2 = \rho_\infty/\varepsilon, \quad u_2 = (1-\varepsilon)u_s \tag{8}$$

Equations (1) and (7) can be written in nondimensional variables

$$S = BT - 0.8T^2 \tag{9}$$

where

$$B = [1/(1-\varepsilon)](\varepsilon/b_\infty)^{1/2}, \quad b_\infty = \rho_\infty/\rho_L \tag{10}$$

This equation has the solution

$$T = (B/1.6)[1 - (1 - 3.2S/B^2)^{1/2}] \tag{11}$$

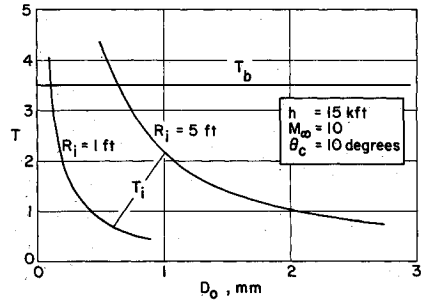

Fig. 7 Impact and breakup times for cone.

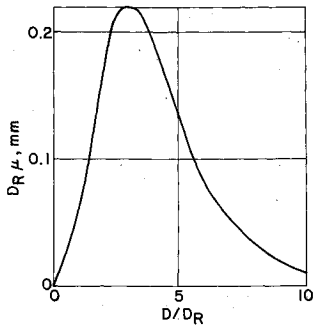

Fig. 8 Rainstorm mass distribution function.

In relating this equation to the case of flight through the atmosphere, we interpret u_s as the flow velocity component normal to the shock wave: in the stagnation region, the freestream velocity V_∞; in the conical-flow region, the velocity component $V_\infty \sin\theta_s$, where θ_s is the inclination of the shock wave. In what follows, we shall be concerned only with conditions at impact on the vehicle surface. In the stagnation region, the nondimensional distance S is then interpreted as Δ/D_0, where Δ is the shock standoff distance, related to the nose radius R_N and the shock density ratio ε by the high-speed correlation[2]

$$\Delta \cong 0.78\varepsilon R_N \tag{12}$$

In the conical-flow region, S is interpreted as the nondimensionalized perpendicular distance from the shock wave to the body $S = L/D_0 = (R_i/D_0)\sin(\theta_s - \theta_C)$, where R_i is the distance from the cone vertex at which the drop strikes the vehicle surface. We can evaluate L by the high-speed correlation[2]

$$L \cong 0.6\varepsilon\theta_s R_i \tag{13}$$

Here θ_C is the inclination of the vehicle surface. For the two regions, Eq. (11) then gives the impact time in the form

$$T_i = \begin{cases} (B/1.6)[1 - (1 - Z_N R_N/D_0)^{1/2}], & \text{Nose} \\ (B/1.6)[1 - (1 - Z_C R_i/D_0)^{1/2}], & \text{Cone} \end{cases} \tag{14}$$

where

$$Z_N = 2.5(1-\varepsilon)^2 b_\infty, \quad Z_C = 1.92(1-\varepsilon)^2 b_\infty \theta_s \tag{15}$$

It is therefore seen that, for given flight conditions and for a given θ_s, the nondimensional impact times are functions only of the ratios R_N/D_0 and R_i/D_0.

The experimental breakup criteria which we have used are as follows: If the impact time T_i is greater than the breakup time T_b, the drop mass at impact is taken to be zero. If the impact time is less than the breakup time, the drop mass at impact is given by the stripping mode correlation (6). The breakup time is taken to be the smaller of 3.5 (stripping mode) and 45 $W^{-1/4}$ (catastrophic mode), where

$$W = \rho_2 u_2^2 D_0/\sigma_L = [(1-\varepsilon)^2/\varepsilon]\, W_\infty \sin^2\theta_s, \qquad W_\infty = \rho_\infty V_\infty D_0/\sigma_l \tag{16}$$

We have considered a flight Mach number $M_\infty = 10$ at 15 kft altitude in the detailed breakup calculation below. At that altitude, there is a peak in the rainstorm water content for the particular model which we chose (described below), so that these

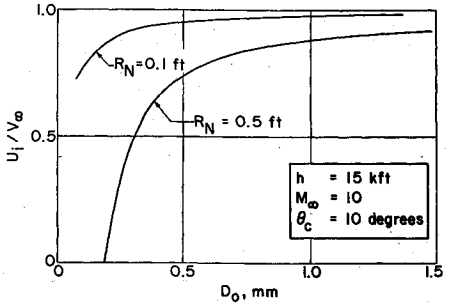

Fig. 9 Impact velocity for nose.

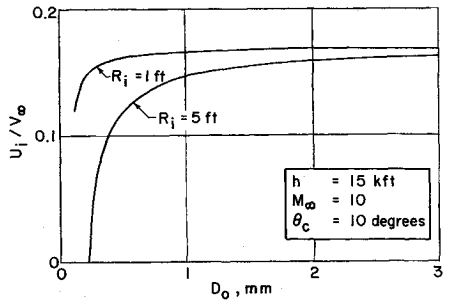

Fig. 10 Normal velocity at impact for cone.

conditions are representative of a severe rain environment. We chose representative nose radii of 0.1 and 0.5 ft, and in the conical-flow region we took a 10 half-angle cone with $R_i = 1$ and 5 ft. (Because of the small cone half-angle, these values essentially designate both the axial and slant location of the impact points.)

Figures 6 and 7 show the impact and breakup times as functions of the initial drop diameter (D_0) in millimeters for the four cases. Figure 6 shows that the breakup time in the nose region can be strongly influenced by the catastrophic mode. We observe that in the nose region, drops with diameters less than 0.07 mm do not reach the surface of the 0.1-ft-radius nose. For the 0.5-ft-radius nose the breakup effect is much more important: the cutoff diameter for complete drop breakup is 0.68 mm, which is twice the cutoff diameter obtained when only the stripping mode of breakup is considered.

In the conical-flow region (see Fig. 7), the stripping mode controls the amount of mass reaching the surface. At the 1-ft station, drops with diameters smaller than 0.12 mm are completely dissipated before they reach the surface, while at the 5-ft station the corresponding diameter is 0.66 mm.

We chose as a rainstorm model a typical summer storm referred to in the Air Force Handbook of Geophysics[8] as case I. The maximum updraft was taken to be 0.2 m/sec yielding a precipitation rate of 0.2 in./hr. The rain concentration is about 1 g/m^3, giving an incoming mass rate of about 0.02 slug/ft^2-sec. The rain concentration will not enter directly into these calculations, however; the results will be given in terms of the mass fraction of the incoming rain that reaches the vehicle surface, so that the impinging mass rate per surface area of the vehicle must be determined by multiplying by the rain concentration, the vehicle velocity and the surface inclination.

Reference 8 (pp. 6–9) gives an expression for the raindrop size distribution function which can be converted into the following mass distribution function:

$$\mu = (1/6D_R)(D/D_R)^3 e^{-D/D_R} \tag{17}$$

Here μdD is the mass fraction of drops with diameters between D and $D + dD$, and the reference diameter D_R is related to the reference diameter D_0 in Ref. 8 by

$$D_R = D_0/3.67 \tag{18}$$

The reference diameter D_R is a weak function of the precipitation rate[8]; in this case, $D_R = 0.255$ mm. This distribution function is shown plotted in Fig. 8.

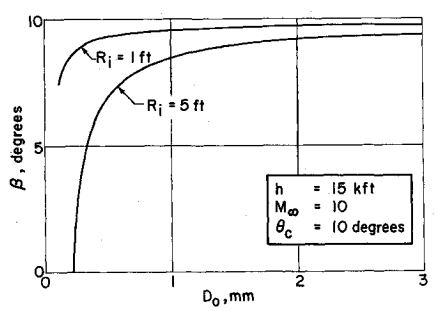

Fig. 11 Impact angle for cone.

Table 1 Results of drop mass removal calculations, $M_\infty = 10$, $h = 15$ kft, $\theta_c = 10°$

	Nose		Cone	
	$R_N = 0.1$	0.5	$R_i = 1$	5 ft
Cutoff diameter D_1, mm	0.07	0.68	0.12	0.66
Minimum drop diameter D_m	0.08	0.39	0.12	0.62
Mass fraction M_1 of drops with $D \geq D_1$	1.00	0.72	1.00	0.74
Net impinging mass fraction M_1	0.98	0.56	0.92	0.29

It should be noted that this model storm takes into account only precipitating rain and neglects the cloud water content, which can be even greater than the precipitating water content. Note that the cloud water is also distributed over much smaller particles, so that the shock layer effect on the cloud water should be more pronounced than on the precipitating water.

The mass fraction of drops with diameters greater than a given diameter D_1 can be determined by integrating Eq. (17)

$$M_1 = \int_{D_1}^{\infty} \mu dD = [1 + \bar{D}_1 + (\bar{D}_1)^2/2 + (\bar{D}_1)^3/6] \exp(-\bar{D}_1)_1 \tag{19}$$

where

$$\bar{D}_1 = D_1/D_R \tag{20}$$

an estimate would disregard the fact that a significant fraction of the drops which do reach the surface have had part of their mass stripped off. The mass fraction of these drops which strikes the surface must be computed by applying Eq. (6) to the mass distribution function and integrating over the remaining drops. The total impinging mass fraction then becomes

$$M_i = \int_{D_1}^{\infty} \frac{m_s}{m_0} \mu dD \tag{21}$$

where D_1 is the drop diameter cutoff for which $T_i = T_b$.

The results of the mass removal calculations are summarized in Table 1. We have tabulated the cutoff diameter D_1 described above and, for comparison, the minimum drop diameter D_m from Eqs. (48) and (49) of Ref. 2 based on Nicholson's data.[3] The drop mass fraction M_i which reaches the surface [Eq. (21)] is shown, together with the mass fraction M_1 of drops with diameters greater than the cutoff diameter D_1 [Eq. (19)]. It is interesting to observe that D_1 and D_m agree quite well in those cases where the catastrophic mode of breakup is relatively unimportant. The difference between the last two rows of Table 1 is attributable to the reduction by stripping of the mass of those drops which strike the surface.

Clearly for the 0.1-ft-radius nose and 1-ft station on the cone the drops lose virtually none of their mass, and the impinging mass on the surface at these points will comprise nearly all the mass which has entered the shock layer at the corresponding points. For the 0.5-ft-radius nose, only about half the entering drop mass strikes the vehicle surface at the stagnation point. At the 5-ft station on the cone, less than a third of the entering drop mass reaches the cone.

Our predictions for drops smaller than 0.5 mm in diameter are based on extrapolations of data obtained for larger drop sizes and hence the predicted breakup behavior for microdrops may be somewhat in error. Additional experimental work is now underway to provide experimental data over a broader range of the parameters and to pin down the critical drop breakup parameters for very small droplets.

Figures 9–11 show drop impact velocities and angles as functions of drop diameter D_0. The drop impact velocity components normal to the body surface were obtained by differentiating the experimental drop trajectory correlation, Eq. (1). The impact angles were obtained from the impact velocity

component normal to the surface together with the component tangential to the surface; the latter is unchanged during passage through the shock layer. Note from these figures and Table I that the cutoff points for total drop breakup occur before a drop has been substantially decelerated or deflected.

Conclusions

Drop breakup effects induced by high-speed shock layers must be accounted for in calculating surface damage caused by raindrops. Depending on the flight conditions and vehicle configuration, a large fraction of the entering drop mass may be dissipated in the shock layer, never reaching the vehicle surface. Based on correlations of recent experimental data, including the actual drop mass removal histories, calculations show that both the stripping and catastrophic breakup modes are important in the vehicle stagnation region. In the downstream conical-flow region, on the other hand, the stripping mode of breakup is dominant. In either case, drop breakup is a much more significant mechanism than deceleration or deflection for protecting the surface of a high-speed vehicle from incoming rain.

References

[1] Ranger, A. and Nicholls, J., "Aerodynamic Shattering of Liquid Drops," *AIAA Journal*, Vol. 7, No. 2, Feb. 1969, pp. 285–290.

[2] Waldman, G. D. and Reinecke, W. G., "Particle Trajectories, Heating and Breakup in Hypersonic Shock Layers," *AIAA Journal*, Vol. 9, No. 6, June 1971, pp. 1040–1048.

[3] Nicholson, J., "Drop Breakup by Airstream Impact," *Rain Erosion and Associated Phenomena*, Rept. N68-19401-427, Royal Aeronautical Establishment, Farnborough, England, 1967.

[4] Engel, O. G., "Fragmentation of Waterdrops in the Zone Behind an Air Shock," *Journal of Research of the NBS*, Vol. 60, No. 3, March 1958, pp. 245–280.

[5] Reinecke, W. G. and Waldman, G. D., "A Study of Drop Breakup Behind Strong Shocks with Applications to Flight," AVSD-0110-70-RR, SAMSO-TR-70-142, May 1970, Avco Corp., Wilmington, Mass.

[6] Reinecke, W. G. and Waldman, G. D., "An Investigation of Water Drop Disintegration in the Region Behind Strong Shock Waves," *3rd International Conference on Rain Erosion and Related Phenomena*, Aug. 1970, Hampshire, England.

[7] Reinecke, W. G. and McKay, W. L., "Experiments on Water Drop Breakup Behind Mach 3 to 12 Shocks," AVATD-0172-69-RR, June 1969, Avco Corp., Wilmington, Mass.

[8] Campen, C. F., Jr. et al., eds., *Handbook of Geophysics*, Revised Edition, Macmillan, New York, 1960.

SEPTEMBER 1972 AIAA JOURNAL VOL. 10, NO. 9

Experimental Investigation of Recirculating Cells in Laminar Coaxial Jets

N. R. WARPINSKI,* H. M. NAGIB,† AND Z. LAVAN‡
Illinois Institute of Technology, Chicago, Ill.

Utilizing several means of introducing smoke into the flowfield for careful visualization in addition to hot-wire techniques, the present investigation establishes the existence of recirculating cells on the axis of laminar circular coaxial mixing jets when the outer jet is substantially faster than the inner one. The experiments are performed in a specially designed facility producing laminar flows up to considerably high Reynolds numbers. The characteristics of the cells and the flow conditions that bring them about are documented by smoke photographs in the Reynolds number-velocity ratio plane and the results are compared to previous analytical predictions. Agreement is found between the theoretically predicted incipient cell formation curve and the one obtained experimentally in spite of the observed unsteadiness of some of the cells. The cells are found to fall into three categories with different flow characteristics involving unsteadiness in position, and shear layer instabilities which result in higher mixing with the outer streams. Qualitative agreement is found between the hot-wire mean velocity measurements and the numerical calculations along the axis of the mixing chamber in the presence of cells.

Nomenclature

d = inner jet diameter $= 2r_i$
d_c = diameter of cylinder used in hot-wire calibration
E = hot-wire bridge-top voltage
E_0 = hot-wire bridge-top voltage at zero velocity
f = frequency of cylinder vortex shedding
G = Grashof number
R_c = Reynolds number of cylinder used in hot-wire calibration
Re = Reynolds number based on the total mass flow rate and the outer jet diameter $= 2\overline{W}r/\nu = Re_j(1 + 15\lambda)/4$
Re_j = inner jet Reynolds number $= 2W_i r_i/\nu = 4Re/(1 + 15\lambda)$
r = radial distance measured from the axis of jet
r_i = inner jet radius
r_o = outer jet radius
S = cylinder shedding Strouhal number $= fd_c/U$
U = mean effective velocity measured by hot-wire
W = local mean velocity in the axial direction
$\overline{W}$ = average axial velocity based on the total mass flow rate
W^* = nondimensional local mean velocity in the axial direction $= W/\overline{W}$
W_i = mass flow average axial velocity of inner jet
W_o = mass flow average axial velocity of outer jet
Z = axial distance measured from the exit plane of the inner jet
Z^* = nondimensional axial distance $= Z/r_o$
λ = velocity ratio $= W_o/W_i$
ν = fluid kinematic viscosity

Presented as Paper 72-150 at the AIAA 10th Aerospace Sciences Meeting, San Diego, Calif., January 17–19, 1972; submitted January 25, 1972; revision received April 19, 1972. Supported by NASA Grant NGR 14-004-008 from the Space Nuclear Propulsion Office. The authors would like to thank A. A. Fejer and M. V. Morkovin for the most stimulating discussions during the course of this investigation. The assistance of U. Mehta and K. Bhatt with the numerical calculations is also appreciated.

Index categories: Jets, Wakes, and Viscid-Inviscid Flow Interaction; Nuclear Propulsion.

* Research Assistant, Mechanics and Mechanical and Aerospace Engineering Department; presently at Mechanical Engineering Department, University of Illinois at Urbana. Student Member AIAA.

† Instructor, Mechanics and Mechanical and Aerospace Engineering Department. Associate Member AIAA.

‡ Associate Professor, Mechanics and Mechanical and Aerospace Engineering Department. Member AIAA.

Introduction

THE mixing of confined coaxial jets has many applications (e.g., jet pumps, thrust augmentors, and ejectors) and has